UC Berkeley
UC Berkeley Previously Published Works

Title
Negative Differential Resistance and Steep Switching in Chevron Graphene Nanoribbon Field-Effect Transistors

Permalink
https://escholarship.org/uc/item/4855j48w

Journal
IEEE Electron Device Letters, 39(1)

ISSN
0741-3106

Authors
Smith, Samuel
Llinás, Juan-Pablo
Bokor, Jeffrey
et al.

Publication Date
2018

DOI
10.1109/led.2017.2772865

Peer reviewed

eScholarship.org Powered by the California Digital Library
University of California

Negative Differential Resistance and Steep Switching in Chevron Graphene Nanoribbon Field-Effect Transistors

Samuel Smith, Juan-Pablo Llinás, Jeffrey Bokor, and Sayeef Salahuddin

***Abstract*— We show that recently fabricated Chevron-type graphene nanoribbons act as a monolithic superlattice structure. This is enabled by the large periodic unit cells with regions of different effective bandgaps in these nanoribbons, resulting in minibands and gaps in the density of states above the conduction band edge. Quantum transport calculations based on non-equilibrium Green's function formalism reveal that a negative differential resistance (NDR) is expected to manifest in these nanoribbons. Due to the relatively low density of states, such NDR behavior can also be modulated with a gate electric field. We show that a sub-thermal subthreshold swing ($<kT/q$) can potentially be obtained in a three-terminal configuration, even in the presence of optical phonon scattering.**

***Index Terms*— Graphene nanoribbons, steep-slope switch, negative differential resistance, quantum transport.**

UNLIKE an Esaki diode, superlattices could provide negative differential resistance without the need of tunneling [1]. Nonetheless, significant difficulty in synthesizing atomically precise, epitaxial heterostructures has made it very challenging to realize such superlattice structures [2]–[8]. In recent years, much work has been done on superlattices involving graphene nanoribbon (GNR) and cabon nanotube (CNT) heterostructure and superlattices and also III-V nanowire heterostructure within the context of steep subthreshold tunnel transistors (TFET) [9]–[18]. However, the difficulty in artificially synthesizing these heterostructures remains. Here, we show that the recently synthesized chevron nanoribbons [19] (CGNR) provide a natural, monolithic material system where superlattice-like narrow-width energy bands and negative differential resistance (NDR) can be achieved. Importantly, the edge roughness that plagues device performance in conventional GNRs [20], [21] can be avoided as it was experimentally demonstrated that such chevron GNRs can be synthesized with atomistically pristine edge states [19], [22]–[24].

Manuscript received October 26, 2017; accepted November 8, 2017. Date of publication November 13, 2017; date of current version December 27, 2017. This work was supported by NSF CAREER under Grant CISE-1149804. The work of J.-P. Llinás and J. Bokor was supported by the Office of Naval Research BRC program under Grant N00014-16-1-2229. The review of this letter was arranged by Editor E. A. Gutiérrez-D. *(Corresponding author: Sayeef Salahuddin.)*

The authors are with the Department of Electrical Engineering and Computer Sciences, University of California at Berkeley, Berkeley, CA 94720 USA (e-mail: sayeef@eecs.berkeley.edu).

Color versions of one or more of the figures in this letter are available online at http://ieeexplore.ieee.org.

Digital Object Identifier 10.1109/LED.2017.2772865

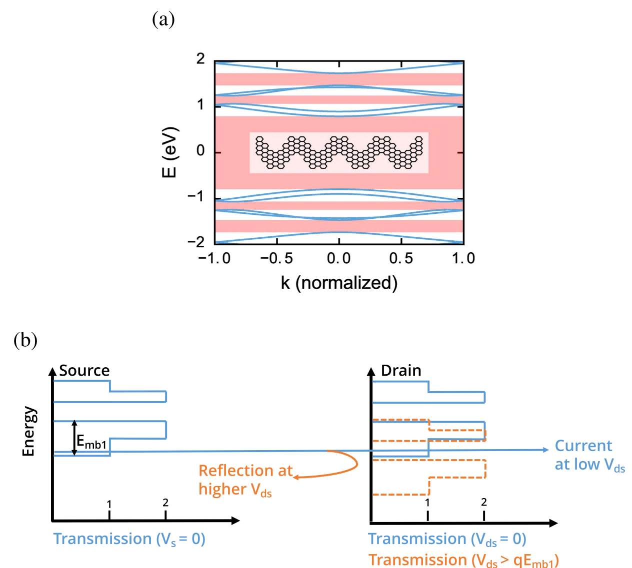

Fig. 1. (a) Band structure of a chevron GNR based on a p_z orbital basis set. The width (and thus quantum confinement) varies across the unit cell, giving a superlattice-like band structure. Forbidden energies are highlighted in red. The bandgap of the ribbon is 1.59 eV, the first conduction band has a bandwidth of 0.272 eV, and the first gap between minibands is 0.178 eV. Inset: Chevron GNR structure. (b) When a gate voltage turns the device ON, current conduction occurs at low values of V_{ds} where the first miniband at the source is aligned with the first miniband at the drain. As the drain voltage is increased beyond qE_{mb1}, the bandwidth of the first miniband, transmission is cut off and the device exhibits NDR.

Fig. 1(a) shows both the structure of the 6-9 CGNR originally fabricated by Cai *et al.* and the band structure calculated with a p_z orbital-based tight-binding method [19]. A key feature of the band structure is the presence of minibands with regions of forbidden energy above the conduction band edge, such as those seen in superlattices of III-V semiconductors. When we look at the CGNR in Fig. 1(a), we see that its narrowest segment is 6 carbon atoms across, and its widest segment is 9 carbon atoms across, with both segments having armchair-type edges. Using a p_z-basis set (GW [25]), the bandgap, E_g, of a 6-AGNR is 1.33 eV (2.7 eV) and the bandgap of a 9-AGNR is 0.95 eV (2.0 eV). However, given the very short length scale over which the width changes in our structure ($\sim$1 nm), one would not expect the system to behave as though the local effective potential oscillates between the bulk values of E_g for the isolated AGNRs. In fact, our chevron structure has an overall bandgap of 1.59 eV.

0741-3106 © 2017 IEEE. Personal use is permitted, but republication/redistribution requires IEEE permission.
See http://www.ieee.org/publications_standards/publications/rights/index.html for more information.

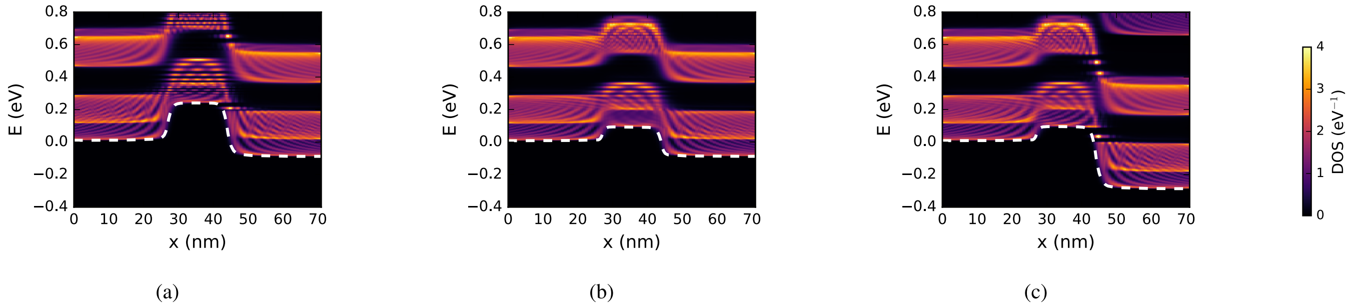

Fig. 2. Local density of states as a function of position and energy. (a) OFF state. Leakage current is reduced because the superlattice gap in the drain filters higher energy electrons, which could otherwise travel over the source-side barrier. (b) ON state. Current is primarily carried by lower energy carriers, which are not blocked by the filtering at the drain. (c) ON state for a higher value of V_{ds}. Significant ballistic transport is no longer possible when the drain voltage is greater than the width of the first miniband minus the height of the source-side barrier. Conduction is only possible through phonon-assisted tunneling.

TABLE I
SIMULATION PARAMETERS

Parameter	Value
Source/Drain doping	1.0×10^{13} cm^{-2}
Channel length	15 nm
Gate contact width $(\perp)$	30 nm
CGNR length	70 nm
Effective oxide thickness	1 nm
p_z hopping energy	2.7 eV
Acoustic phonon coupling, $D_{\omega,AP}$	0.01 eV^2
Optical phonon coupling, $D_{\omega,OP}$	0.01 eV^2
Optical phonon energy, $\hbar\omega_{OP}$	196 meV

This value is consistent with the 1.62 eV bandgap from LDA DFT calculations, but significantly smaller than the 3.74 eV value from calculations incorporating the GW correction [26]. Both LDA and GW calculations show the presence of minibands and gaps above the conduction band edge [26]. We also calculated the CGNR band structure with the *pd* tight-binding model of Boykin *et al.* [27] and find good agreement with the results obtained from p_z basis set.

Within this model, the bandgap was 1.50 eV and the width of the first miniband for the conduction band was 71 meV, lower than the 272 meV value for the p_z Hamiltonian. However the width of the first miniband in the valence band was 314 meV, consistent with the bandwidth in p_z model, which is symmetric for conduction and valence bands. The gap between the first and second of minibands was 187 meV for the valence band and 295 meV for the conduction band, compared with 178 meV for the p_z model.

Simulations are performed on a double gate MOSFET geometry using the non-equilibrium Green's function (NEGF) formalism [28]. A simple p_z-basis Hamiltonian with hopping parameter $t_0 = 2.7\,eV$ is used. The NEGF equations are solved self-consistently with the nonlinear Poisson equation in three dimensions. Acoustic and optical phonon scattering are taken into account with the according to the method described in [29]–[33]. Because we lack an exact values for the electron-phonon coupling constants, we use approximate values similar to those used by Koswatta *et al.* [30] for CNTs. The simulation parameters are shown in TABLE I.

Operation differs from a MOSFET in two key ways. The first is that the device shows NDR with respect to the drain voltage. Fig. 1(b) illustrates this phenomenon. At low drain biases, conduction will occur within the first miniband. When the drain voltage is increased to the point where the gap above the first miniband at the drain is aligned with the source Fermi level, conduction is cut off. With even higher drain voltage, band-to-band tunneling from the first miniband to the second miniband becomes possible, and current increases again. The second feature of the device is that the superlattice gap at the drain filters out higher energy electrons from the first miniband at the source when a source-drain bias is applied. This cuts off the higher energy portion of the Fermi function at the source, resulting in energy filtering as in a TFET. Transport in this device, however, is entirely intraband like a MOSFET, whereas a TFET relies on band-to-band tunneling. This could possibly allow higher ON current than a TFET.

The CGNR used in our simulation has a width of 1.9 nm. The simulation domain is approximately 70 nm long, and the gate has a length of 15 nm. The source and drain are doped with $N_D = 1.0 \times 10^{13}$ cm^{-2} donors. An effective oxide thickness of 1.0 nm is used for both the top and bottom gates. The gate contacts are extended 30 nm perpendicular to the channel to capture fringing gate fields. While our simulation uses an effective doping density to align the source and drain Fermi levels to the CGNR conduction band, this could be achieved in an experiment through electrostatics alone. The parameters for the simulation are listed in Table I.

The local density of states for the CGNR MOSFET is shown in Fig. 2 for several biasing conditions. Fig. 2b shows peak current case when a large enough drain bias has been applied to generate enough splitting between the source and drain Fermi levels to allow significant current to flow, but not a high enough bias to move the first miniband outside of the current conduction window. In this case, as is shown in Fig.3, nearly all conduction occurs solely through phonon-assisted tunneling. For higher bias as in Fig. 2c, intraband conduction from the first miniband is completely cut off, though a significant current continues to flow because of optical phonon scattering. As the drain bias is further increased, current can only flow due to band-to-band tunneling from the first miniband at the source to the second miniband at the drain or through phonon-assisted tunneling. Note that, due to the minibands, there will be regions of operation for both gate and drain voltages where direct current flow is abruptly turned on or off, as the overlap between source minibands and

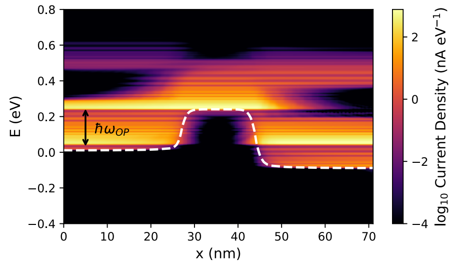

Fig. 3. Energy-resolved current spectrum at $V_{gs} = 0.55$ V, $V_{ds} = 0.10$ V. Optical phonon scattering couples minibands that would not be coupled in ballistic transport, thereby degrading both subthreshold swing and NDR.

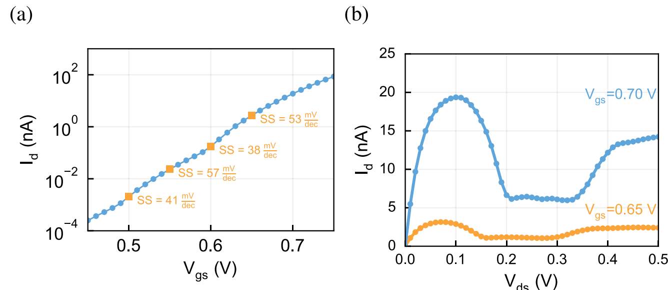

Fig. 4. (a) $I_{ds} - V_{gs}$ for $V_{ds} = 0.1$ V. Steep-slope behavior is observed with a subthreshold swing of around of 49 mV/decade over four decades of current between $V_{gs} = 0.48$ V and $V_{gs} = 0.68$ V with a minimum value of 38 mV/decade around $V_{gs} = 0.60$ V. (b) Ids - Vds for two values of Vgs. When $V_{gs} = 0.7$ V, a peak-to-valley ratio of 3.15 is achieved.

drain minibands is modified. This leads to a steep subthreshold swing (< 60 mV/decade at room temperature) in the $I_{ds} - V_{gs}$ characteristic and a negative differential resistance in the $I_{ds} - V_{ds}$ characteristic.

Fig. 4(a) shows I_{ds} vs. V_{gs} for $V_{ds} = 0.1$ V. While steep-slope behavior is exhibited at some point for all values of V_{ds}, the highest ON current is observed for $V_{ds} = 0.1$ V. At this drain bias, an ON current of 85 nA is achieved at a gate bias of $V_{gs} = 0.75$ V. The subthreshold swing is 49 mV/decade when averaged over four orders of magnitude of I_{ds} between $V_{gs} = 0.48$ V and $V_{gs} = 0.68$ V at $V_{ds} = 0.1$ V with a minimum value of 38 mV/decade around $V_{gs} = 0.60$ V. Over this range of 0.2 V, the ON-OFF ratio is 2.1×10^6. With gate work function engineering and additional device optimization, it should be possible to achieve reasonable ON current with a low supply voltage. The origin of the steep-slope behavior can be understood from Fig. 2. In the OFF state shown in Fig. 2a, the superlattice gap at the drain prevents leakage current from flowing over the source-side injection barrier. The states near the top of the barrier are seen to decay rapidly in the drain region. Fig. 2b shows the ON state, in which low-energy electrons, which make up virtually all of the ON current, can flow unimpeded from source to drain.

The $I_{ds} - V_{ds}$ curves are shown in Fig. 4(b). When $V_{gs} = 0.7$ V, we see an increase in current up to $V_{ds} = 0.10$ V. As the drain bias is further increased, we see a decrease in current as the drain miniband goes out of alignment with the source miniband. The current begins to pick up again as the second miniband at the drain comes in alignment with the source miniband again. The peak-to-valley ratio (PVR) at this gate voltage is 3.15. At $V_{gs} = 0.65$ V, the calculated PVR is 2.89.

Figure 3 shows the energy-resolved current spectrum in the OFF state at $V_{gs} = 0.55$ V, $V_{ds} = 0.10$ V (the same bias point as Fig. 2a). In the OFF-state, subthreshold leakage current is suppressed because of the lack of states at the drain at the energy of the top of the barrier. However, optical phonon scattering permits some carriers to be scattered down into the first miniband at the drain. Nevertheless, the steep-slope behavior is preserved, despite being deteriorated relative to 6 mV/decade subthreshold swing observed in ballistic calculations. Previously, Yoon and Salahuddin [33] studied the effects of phonon-assisted band-to-band tunneling in AGNR tunnel transistors. That work concluded that while subthreshold swing in those devices was degraded by electron-phonon scattering, it was still possible to achieve a subthreshold swing of 34 mV/decade, far below the Boltzmann limit, consistent with the degradation in performance we see in our device when the effects of the electron-phonon interaction are considered.

Previous work on III-V MOSFETs with a superlattice source filter by Lam *et al.* [34] found that it should be possible to achieve $I_{ON} = 0.81$ mA μm^{-1} with $SS = 20.9$ mV/decade at $V_{ds} = 0.6$ V, though this calculation did not take into account phonon scattering. Assuming a device with multiple ribbons in parallel with a pitch of 5 nm, our device achieves $I_{ON} = 0.017$ mAμm^{-1}. While this value is much smaller, our device operates $V_{ds} = 0.1$ V. Because of the NDR effect, higher drain biases unfortunately result in lower current.

In summary, we have shown that CGNR devices can exhibit both steep-slope subthreshold behavior and negative differential resistance. Both properties are the result of the superlattice-like electronic structure of the ribbon. CGNR SLFETs could be promising for a number of applications ranging from low-power logic transistors to high speed oscillators. A major obstacle to building a real device is making contacts with appropriate Schottky barrier heights to be able to match the band alignment conditions achieved in this work through doping. The performance of a real device could also be impacted by edge roughness, which we have not considered here, though the ability to synthesize ribbons with virtually no defects may minimize this effect. Additional optimization is also likely necessary to make a functioning device. DFT+GW calculations predict a much higher bandgap for the CGNR in vacuum than the tight-binding model used in this work. While surface screening may reduce the bandgap, a wider ribbon with a narrower bandgap may be required. Co-optimization of the bandgap with the bandwidths of the minibands and the gaps between minibands is also a necessary topic for future work.

Acknowledgment

The authors would like to acknowledge insightful discussions with Felix Fischer and Mike Crommie.

References

[1] L. Esaki and R. Tsu, "Superlattice and negative differential conductivity in semiconductors," *IBM J. Res. Develop.*, vol. 14, no. 1, pp. 61–65, 1970, doi: 10.1147/rd.141.0061.

[2] L. Esaki and L. Chang, "New transport phenomenon in a semiconductor 'superlattice,'" *Phys. Rev. Lett.*, vol. 33, no. 8 p. 495, 1974, doi: 10.1103/PhysRevLett.33.495.

[3] K. Choi, B. Levine, R. Malik, J. Walker, and C. Bethea, "Periodic negative conductance by sequential resonant tunneling through an expanding high-field superlattice domain," *Phys. Rev. B, Condens. Matter*, vol. 35, no. 8, p. 4172, 1987, doi: 10.1103/PhysRevB.35.4172.

[4] K. Ismail, W. Chu, A. Yen, D. A. Antoniadis, and H. I. Smith, "Negative transconductance and negative differential resistance in a grid-gate modulation-doped field-effect transistor," *Appl. Phys. Lett.*, vol. 54, no. 5, pp. 460–462, Jan. 1989, doi: 10.1063/1.100952.

[5] G. Bernstein and D. Ferry, "Negative differential conductivity in lateral surface superlattices," *J. Vac. Sci. Technol. B, Microelectron. Process. Phenomena*, vol. 5, no. 4, pp. 964–966, 1987, doi: 10.1116/1.583699.

[6] H. Grahn, R. Haug, W. Müller, and K. Ploog, "Electric-field domains in semiconductor superlattices: A novel system for tunneling between 2D systems," *Phys. Rev. Lett.*, vol. 67, no. 12, p. 1618, 1991, doi: 10.1103/PhysRevLett.67.1618.

[7] J. Kastrup, H. Grahn, K. Ploog, F. Prengel, A. Wacker, and E. Schöll, "Multistability of the current-voltage characteristics in doped GaAs-AlAs superlattices," *Appl. Phys. Lett.*, vol. 65, no. 14, pp. 1808–1810, 1994, doi: 10.1063/1.112850.

[8] A. Warren, D. Antoniadis, H. I. Smith, and J. Melngailis, "Surface superlattice formation in silicon inversion layers using 0.2-μm period grating-gate electrodes," *IEEE Electron Device Lett.*, vol. EDL-6, no. 6, pp. 294–296, Jun. 1985, doi: 10.1109/EDL.1985.26130.

[9] G. J. Ferreira, M. N. Leuenberger, D. Loss, and J. C. Egues, "Low-bias negative differential resistance in graphene nanoribbon superlattices," *Phys. Rev. B, Condens. Matter*, vol. 84, no. 12, p. 125453, 2011, doi: 10.1103/PhysRevB.84.125453.

[10] S. Li, C. K. Gan, Y.-W. Son, Y. P. Feng, and S. Y. Quek, "Low-bias negative differential resistance effect in armchair graphene nanoribbon junctions," *Appl. Phys. Lett.*, vol. 106, no. 1, p. 013302, 2015, doi: 10.1063/1.4905269.

[11] H. Teong, K.-T. Lam, S. B. Khalid, and G. Liang, "Shape effects in graphene nanoribbon resonant tunneling diodes: A computational study," *J. Appl. Phys.*, vol. 105, no. 8, p. 084317, 2009, doi: 10.1063/1.3115423.

[12] H. Sevinçli, M. Topsakal, and S. Ciraci, "Superlattice structures of graphene-based armchair nanoribbons," *Phys. Rev. B, Condens. Matter*, vol. 78, no. 24, p. 245402, Dec. 2008, doi: 10.1103/PhysRevB.78.245402.

[13] M. Sharifi, E. Akhoundi, and H. Esmaili, "Negative differential resistance in new structures based on graphene nanoribbons," *J. Comput. Electron.*, vol. 15, no. 4, pp. 1361–1369, 2016, doi: 10.1007/s10825-016-0929-8.

[14] G. Saha, A. K. Saha, and A. H.-U. Rashid, "Double quantum well resonant tunneling negative differential resistance device design using graphene nanoribbons," in *Proc. IEEE 15th Int. Conf. Nanotechnol. (IEEE-NANO)*, Jun. 2015, pp. 440–443, doi: 10.1109/NANO.2015.7388632.

[15] E. C. Girao, E. Cruz-Silva, and V. Meunier, "Electronic transport properties of assembled carbon nanoribbons," *ACS Nano*, vol. 6, no. 7, pp. 6483–6491, 2012, doi: 10.1021/nn302259f.

[16] S. Kim, M. Luisier, T. B. Boykin, and G. Klimeck, "Computational study of heterojunction graphene nanoribbon tunneling transistors with pd orbital tight-binding method," *Appl. Phys. Lett.*, vol. 104, no. 24, p. 243113, 2014, doi: 10.1063/1.4884199.

[17] Y. Yoon and S. Salahuddin, "Barrier-free tunneling in a carbon heterojunction transistor," *Appl. Phys. Lett.*, vol. 97, no. 3, p. 033102, 2010, doi: 10.1063/1.3431661.

[18] E. Gnani, P. Maiorano, S. Reggiani, A. Gnudi, and G. Baccarani, "Performance limits of superlattice-based steep-slope nanowire FETs," in *IEDM Tech. Dig.*, Dec. 2011, pp. 5.1.1–5.1.4, doi: 10.1109/IEDM.2011.6131491.

[19] J. Cai, P. Ruffieux, R. Jaafar, M. Bieri, T. Braun, S. Blankenburg, M. Muoth, A. P. Seitsonen, M. Saleh, X. Feng, K. Müllen, and R. Fasel, "Atomically precise bottom-up fabrication of graphene nanoribbons," *Nature*, vol. 466, no. 7305, pp. 470–473, 2010, doi: 10.1038/nature09211.

[20] G. Fiori and G. Iannaccone, "Simulation of graphene nanoribbon field-effect transistors," *IEEE Electron Device Lett.*, vol. 28, no. 8, pp. 760–762, Aug. 2007, doi: 10.1109/LED.2007.901680.

[21] Y. Yoon and J. Guo, "Effect of edge roughness in graphene nanoribbon transistors," *Appl. Phys. Lett.*, vol. 91, no. 7, pp. 073103-1–073103-13, 2007, doi: 10.1063/1.2769764.

[22] J. P. Llinas, A. Fairbrother, G. B. Barin, W. Shi, K. Lee, S. Wu, B. Y. Choi, R. Braganza, J. Lear, and N. Kau, "Short-channel field-effect transistors with 9-atom and 13-atom wide graphene nanoribbons," *Nature Commun.*, vol. 8, no. 1, p. 633, 2017, doi: 10.1038/s41467-017-00734-x.

[23] J. Cai, C. A. Pignedoli, L. Talirz, P. Ruffieux, H. Söde, L. Liang, V. Meunier, R. Berger, R. Li, X. Feng, K. Müllen, and R. Fasel, "Graphene nanoribbon heterojunctions," *Nature Nanotechnol.*, vol. 9, no. 11, pp. 896–900, 2014, doi: 10.1038/nnano.2014.184.

[24] Y.-C. Chen *et al.*, "Molecular bandgap engineering of bottom-up synthesized graphene nanoribbon heterojunctions," *Nature Nanotechnol.*, vol. 10, no. 2, pp. 156–160, Jan. 2015, doi: 10.1038/nnano.2014.307.

[25] L. Yang, C.-H. Park, Y.-W. Son, M. L. Cohen, and S. G. Louie, "Quasiparticle energies and band gaps in graphene nanoribbons," *Phys. Rev. Lett.*, vol. 99, no. 18, p. 186801, Nov. 2007, doi: 10.1103/PhysRevLett.99.186801.

[26] S. Wang and J. Wang, "Quasiparticle energies and optical excitations in chevron-type graphene nanoribbon," *J. Phys. Chem. C*, vol. 116, no. 18, pp. 10193–10197, 2012, doi: 10.1021/jp2125872.

[27] T. B. Boykin, M. Luisier, G. Klimeck, X. Jiang, N. Kharche, Y. Zhou, and S. K. Nayak, "Accurate six-band nearest-neighbor tight-binding model for the π-bands of bulk graphene and graphene nanoribbons," *J. Appl. Phys.*, vol. 109, no. 10, p. 104304, 2011, doi: 10.1063/1.3582136.

[28] S. Datta, *Quantum Transport: Atom to Transistor*. Cambridge, U.K.: Cambridge Univ. Press, 2005.

[29] H. Pal, D. Nikonov, and G. Bourianoff, "Scattering in NEGF: Made simple," Intel Corporation, Santa Clara, CA, USA, 2009. [Online]. Available: https://nanohub.org/resources/7772

[30] S. O. Koswatta, S. Hasan, M. S. Lundstrom, M. P. Anantram, and D. E. Nikonov, "Nonequilibrium Green's function treatment of phonon scattering in carbon-nanotube transistors," *IEEE Trans. Electron Devices*, vol. 54, no. 9, pp. 2339–2351, Sep. 2007, doi: 10.1109/TED.2007.902900.

[31] Y. Ouyang, X. Wang, H. Dai, and J. Guo, "Carrier scattering in graphene nanoribbon field-effect transistors," *Appl. Phys. Lett.*, vol. 92, no. 24, p. 243124, 2008, doi: 10.1063/1.2949749.

[32] Y. Yoon, D. E. Nikonov, and S. Salahuddin, "Role of phonon scattering in graphene nanoribbon transistors: Nonequilibrium green's function method with real space approach," *Appl. Phys. Lett.*, vol. 98, no. 20, p. 203503, 2011, doi: 10.1063/1.3589365.

[33] Y. Yoon and S. Salahuddin, "Dissipative transport in rough edge graphene nanoribbon tunnel transistors," *Appl. Phys. Lett.*, vol. 101, no. 26, p. 263501, 2012, doi: 10.1063/1.4772532.

[34] K.-T. Lam, Y.-C. Yeo, and G. Liang, "Performance comparison of III-V MOSFETs with source filter for electron energy," in *IEDM Tech. Dig.*, Dec. 2012, pp. 17–6, doi: 10.1109/IEDM.2012.6479062.